JACS
JOURNAL OF THE AMERICAN CHEMICAL SOCIETY
pubs.acs.org/JACS
Article

Structure Responsible for the Superconducting State in $La_3Ni_2O_7$ at High-Pressure and Low-Temperature Conditions

Luhong Wang,* Yan Li, Sheng-Yi Xie, Fuyang Liu, Hualei Sun, Chaoxin Huang, Yang Gao, Takeshi Nakagawa, Boyang Fu, Bo Dong, Zhenhui Cao, Runze Yu, Saori I. Kawaguchi, Hirokazu Kadobayashi, Meng Wang,* Changqing Jin, Ho-kwang Mao, and Haozhe Liu*

Cite This: J. Am. Chem. Soc. 2024, 146, 7506−7514
Read Online
ACCESS | Metrics & More | Article Recommendations | Supporting Information

ABSTRACT: Very recently, a new superconductor with T_c = 80 K has been reported in nickelate ($La_3Ni_2O_7$) at around 15−40 GPa conditions (Nature, 621, 493, 2023), which is the second type of unconventional superconductor, besides cuprates, with T_c above liquid nitrogen temperature. However, the phase diagram plotted in this report was mostly based on the transport measurement under low-temperature and high-pressure conditions, and the assumed corresponding X-ray diffraction (XRD) results were carried out at room temperature. This encouraged us to carry out in situ high-pressure and low-temperature synchrotron XRD experiments to determine which phase is responsible for the high T_c state. In addition to the phase transition from the orthorhombic *Amam* structure to the orthorhombic *Fmmm* structure, a tetragonal phase with the space group of *I*4/*mmm* was discovered when the sample was compressed to around 19 GPa at 40 K where the superconductivity takes place in $La_3Ni_2O_7$. The calculations based on this tetragonal structure reveal that the electronic states that approached the Fermi energy were mainly dominated by the e_g orbitals ($3d_{z^2}$ and $3d_{x^2-y^2}$) of Ni atoms, which are located in the oxygen octahedral crystal field. The correlation between T_c and this structural evolution, especially Ni−O octahedra regularity and the in-plane Ni−O−Ni bonding angles, is analyzed. This work sheds new light to identify what is the most likely phase responsible for superconductivity in double-layered nickelate.

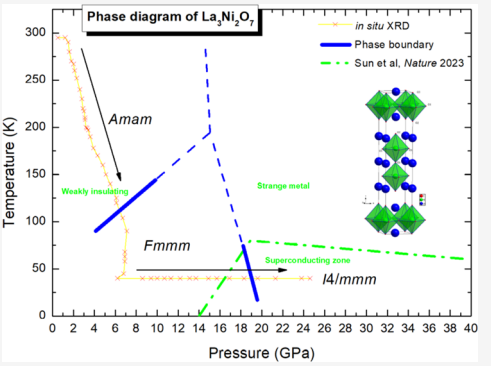

INTRODUCTION

When the result of electrical properties in nickelate $La_3Ni_2O_{7+\delta}$ under high-pressure conditions up to 18.5 GPa was reported at the 21st AIRAPT conference at Catania, Italy in Sep. 2007,[1] it did not attract much attention due to the result that indicated pressure-induced enhancement of the insulating phase. Drama occurred after 16 years when the signature of superconductivity near 80 K in this exact nickelate system under high pressure was reported online in July, 2023,[2] in which high-quality single-crystal samples were synthesized after many years of efforts,[3] and the electronic occupancy of $Ni^{2.5}$ in this Ruddlesden−Popper double-layered perovskite nickelate $La_3Ni_2O_7$ might to some extent mimic the Cu^{2+} of hole-doped bilayer high T_c cuprates, indicating that the nickel-oxide system enables the study of high T_c superconductors and helps in understanding its unconventional high T_c superconductivity mechanism. However, the phase diagram in this sample that was plotted in the recent Nature paper was mainly based on the transport measurement under low-temperature and high-pressure conditions. The assumed corresponding high-pressure X-ray diffraction (XRD) experiments were carried out at room temperature, which was not in the P−T domains of this sample's superconducting state. The follow-up bilayer two-orbital model mechanism investigations were based on this room-temperature high-pressure structure,[4,5] which might not be fastidiously proper if calculations and analysis were based on the crystalline structure at room temperature. Geisler et al. calculated the whole group of $A_3Ni_2O_7$ (A = La−Lu, Y, Sc) as a function of pressure up to 150 GPa and proposed smaller A site cation compound $Tb_3Ni_2O_7$ in the lower symmetry *Cmc*21 structure as a candidate for superconductivity at ambient pressure.[6] In contrast, structural routes to stabilize superconducting $La_3Ni_2O_7$ at ambient pressure were calculated using density functional theory (DFT) structural relaxation based on the room-temperature high-pressure *Fmmm* structure model and then proposed the routes via increasing the size of the A site cation.[7] Theoretical predictions seem to hedge off here and might be pointing in an inaccurate direction, and many eager experimentalists in this field might be confused. Therefore, the in situ synchrotron X-ray diffraction experiments for this nickelate compound at the low-temperature

Received: November 22, 2023
Revised: January 28, 2024
Accepted: February 6, 2024
Published: March 8, 2024

https://doi.org/10.1021/jacs.3c13094
J. Am. Chem. Soc. 2024, 146, 7506−7514

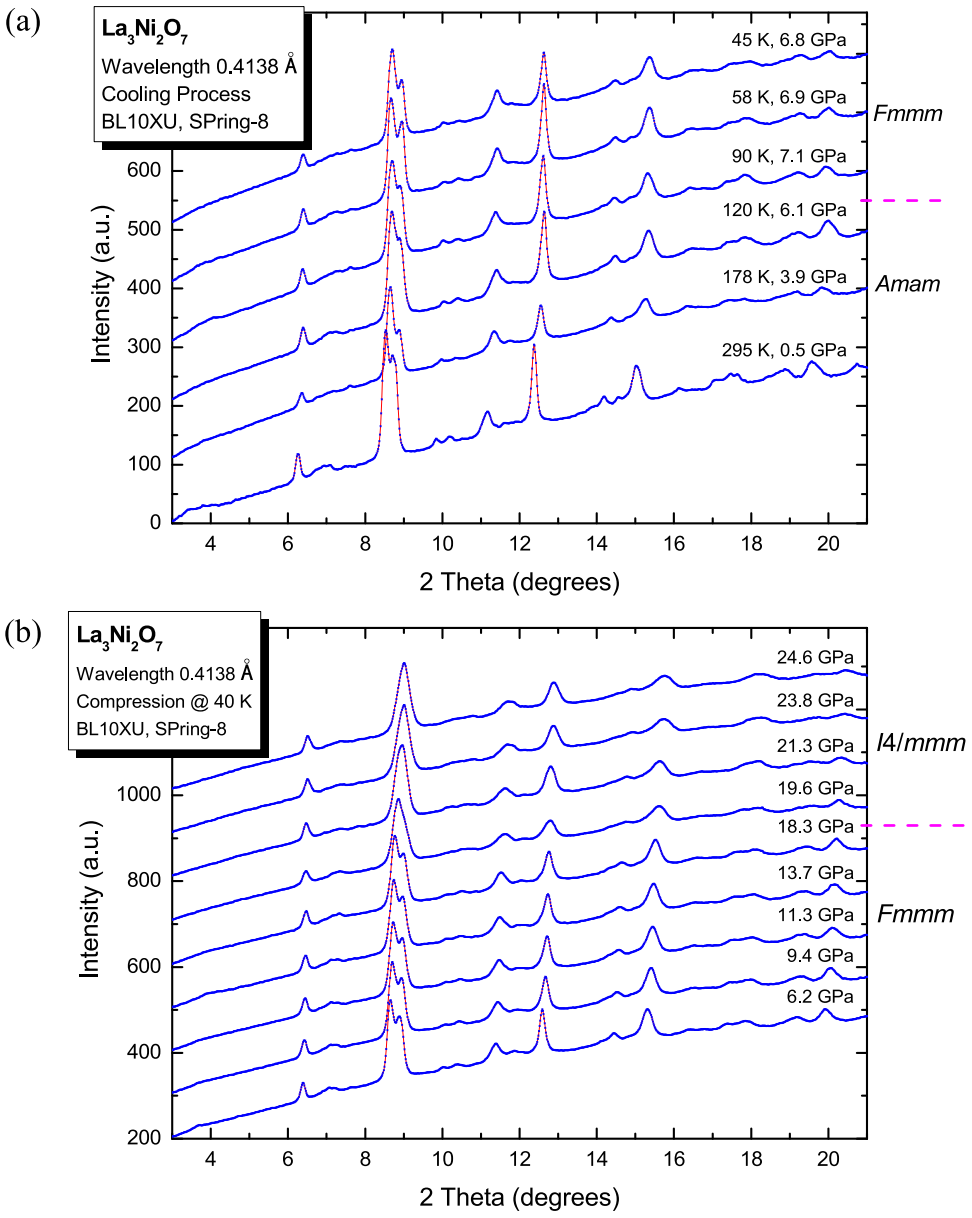

Figure 1. Selected typical XRD patterns during the (a) cooling process and (b) compression process at 40 K.

region, i.e., at the below 80 K region, and pressures above 15 GPa, were carried out to check the phase transition sequence and phase boundaries and to determine which phase is responsible for record high T_c in this nickelate compound.

EXPERIMENTAL AND CALCULATION DETAILS

The in situ high-pressure synchrotron X-ray diffraction experiments were carried out at BL10XU, SPring-8, Japan, with a wavelength of 0.4138 Å. The powder sample, which was ground from a prechecked high-quality single-crystal $La_3Ni_2O_7$ sample, was loaded into a sample chamber of the BeCu-based diamond anvil cell (DAC) with an anvil culet size of 300 μm. The details of sample syntheses were reported previously.[2,3] T301 stainless steel was used as a gasket, and silicone oil was used as a pressure medium. A tiny Au foil was loaded near the sample chunk and used as an internal pressure marker.[8−10] The DAC was mounted into the online cryostat system and fully vacuumed before cooling down. A helium membrane gas control system was used to control pressure remotely. The beam size was focused down to about 10 μm at the sample location. The typical XRD exposure time was 1 s. Diffraction images were integrated using DIOPTAS,[11] and the structural analysis and refinements were performed through the GASA-II package.[12]

The structural relaxations and total energy calculations were adopted with density functional theory (DFT), which was implanted in the Vienna Ab initio Simulation Package (VASP).[13] The projector augmented wave (PAW) pseudopotential[14] with an energy cutoff of up to 600 eV was chosen to describe the electron−ion interaction. The Perdew−Burke−Ernzerhof (PBE) functional[15] with the generalized gradient approximation (GGA) was used to calculate the exchange−correlation interaction between electrons. An effective Hubbard U value of 4 eV was considered in the electronic structure calculation, the same as the previous related calculation setup.[2]

RESULTS AND DISCUSSION

The sample in DAC was compressed to about 1.2 GPa at room temperature, and then the decreasing temperature process was performed while collecting the XRD patterns. The typical XRD patterns during this cooling process are shown in Figure 1a. When the temperature reached 40 K and was maintained at this temperature for over 40 min, the gas membrane control

https://doi.org/10.1021/jacs.3c13094
J. Am. Chem. Soc. 2024, 146, 7506−7514

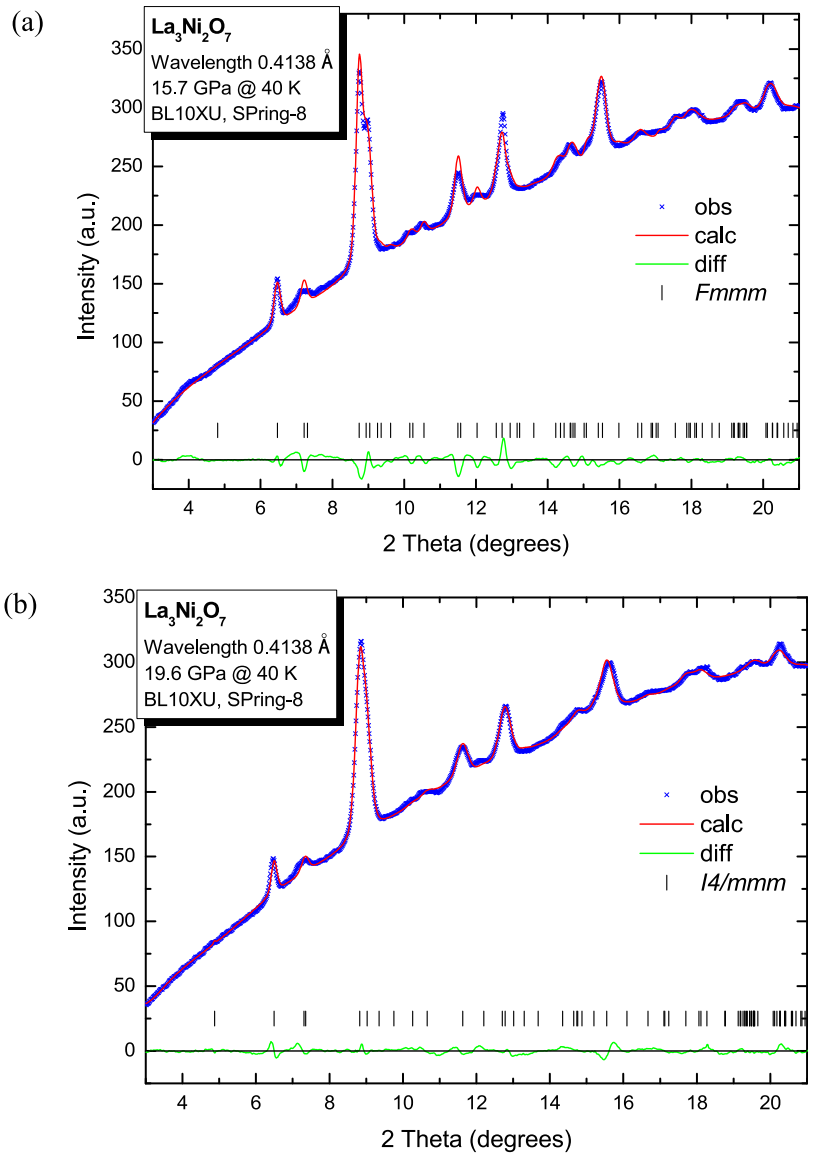

Figure 2. (a) Typical XRD refinement result for the *Fmmm* phase at 15.7 GPa and 40 K, R_w = 1.164%. (b) The typical XRD refinement result for the *I*4/*mmm* phase at 19.6 GPa and 40 K, R_w = 0.656%.

compression process started increasing pressure slowly, and the typical XRD patterns during this compression process are demonstrated in Figure 1b.

A phase transition was observed when cooling down between 120 and 104 K under pressure conditions, starting from the orthorhombic *Amam* structure (space group #63, Z = 4) to the orthorhombic *Fmmm* structure (space group #69, Z = 4). The typical Rietveld refinement based on this *Fmmm* structure for the XRD pattern at 15.7 GPa and 40 K is plotted in Figure 2a.

When the temperature was maintained at 40 K, a tetragonal phase with the space group of *I*4/*mmm* (space group #139, Z = 2) was discovered when the compression was around 19 GPa. We also performed DFT calculations and confirmed that the *I*4/*mmm* structure was stable at pressures above 20 GPa, and the calculated optimized atomic positions in the *I*4/*mmm* structure were used as the starting values in the XRD refinement for this tetragonal phase. The typical Rietveld refinement based on this tetragonal structure for the XRD pattern at 19.6 GPa and 40 K is plotted in Figure 2b.

This nickelate $La_3Ni_2O_7$ belongs to the so-called Ruddlesden−Popper (RP) series (when n = 2) $A_{n+1}B_nC_{3n+1}$ compounds, where A is usually a rare-earth, alkaline-earth or alkali ion, B can be a 3d or 4d transition metal, and C could be fluorine or oxygen. These RP series compounds are layered perovskites separated by a rock-salt structure layer, as shown in Figure 3 for the n = 2 case; therefore, the chemical formula could be written as $(ABC_3)_n(AC)$. The research studies on this crystal family were initiated in the 1950s, and the very early structure found in compound $Sr_3Ti_2O_7$ was indeed the *I*4/*mmm* structure;[16] the exact structure corresponds to the superconducting zone in nickelate $La_3Ni_2O_7$. This tetragonal structure is considered a high-symmetry parent structure in RP compounds, and it has many low-symmetry subgroup structures with the constraint of rigid BC_6 octahedra using the Landau expansion.[17] At ambient conditions, the *Fmmm* structure normally is the popular type in RP compounds,[18] and the nickelate $La_3Ni_2O_7$ was originally synthesized and assigned as the *Fmmm* structure based on XRD data.[19] However, in 1999, a high-resolution neutron diffraction experiment

https://doi.org/10.1021/jacs.3c13094
J. Am. Chem. Soc. 2024, 146, 7506−7514

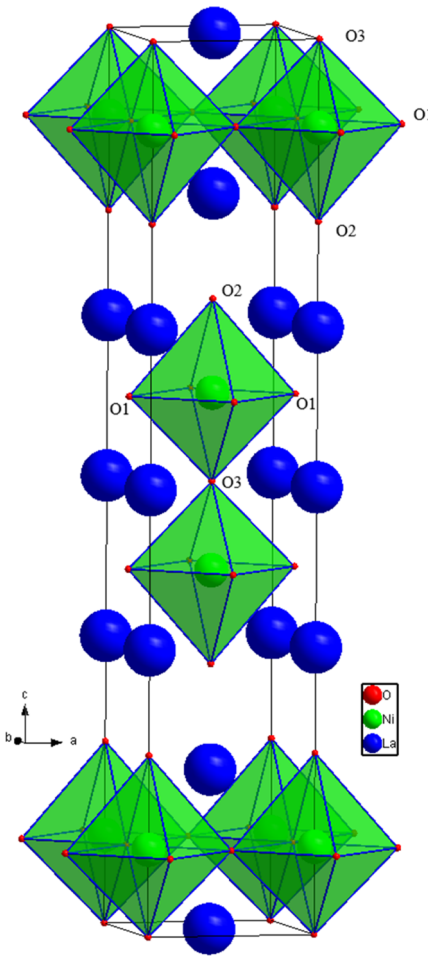

Figure 3. Unit cell ($Z = 2$) of the $I4/mmm$ structure for $La_3Ni_2O_7$.

improved our understanding of this $La_3Ni_2O_7$ structure. Due to some tiny diffraction peaks that could not be explained based on the *Fmmm* structure model, Ling et al. solved its structure using the *Fmmm* structure's subgroup: *Amam* structure.[20] The *Amam* structure setting was chosen, instead of the standard *Cmcm* structure, to let the long axis as the *c* direction, making it relatively easy to compare with its potential higher symmetry parent structure, although the *Cmcm* setting was used in some previous literature studies for $La_3Ni_2O_7$.[3]

The single-crystal XRD experiments at room temperature were also performed using a lab-based silver source Bruker *D*8 Venture diffractometer at HPSTAR. Although the multiple twins and severe texture development easily occur when increasing pressure during multiple runs, the symmetric analysis indeed favors the $I4/mmm$ structure model at pressures above 15 GPa at room temperature. Therefore, the updated phase diagram is plotted based on these in situ XRD results under high pressure at 40 K and room temperature conditions, as shown in Figure 4, in which the solid blue lines indicate the phase boundaries and the extended blue dashed lines as phase boundaries and the possible triple point were guides for the eye. This not only provides the updated phase diagram for this nickelate at low-T and high-P domains but also unveils these record-setting superconductivity and the correct responsible high-pressure phase. This opens up new possibilities for finding more materials that exhibit pressure-driven superconductivity with similar or much higher T_c values than those previously believed achievable in similar systems.

One follow-up question is how to achieve the tetragonal structure in the nickelates via replacement or doping of other elements at the A site to make the potential high T_c materials in this nickelate family become available at ambient conditions. From the point of view of the A/B atomic size ratio in these RP compounds, for example, the very first report tetragonal phase for $Sr_3Ti_2O_7$,[16] the atomic size ratio Sr/Ti = 200:140 = 1.429. For this case, La/Ni = 195:135 = 1.444, indicating that a smaller size atom at the A site might enable stabilization of the $I4/mmm$ structure at ambient conditions. One well-studied system, $La_{2-2x}Sr_{1+2x}Mn_2O_7$, with the same RP structure ($n = 2$) and the tetragonal and orthorhombic phases could be tuned by

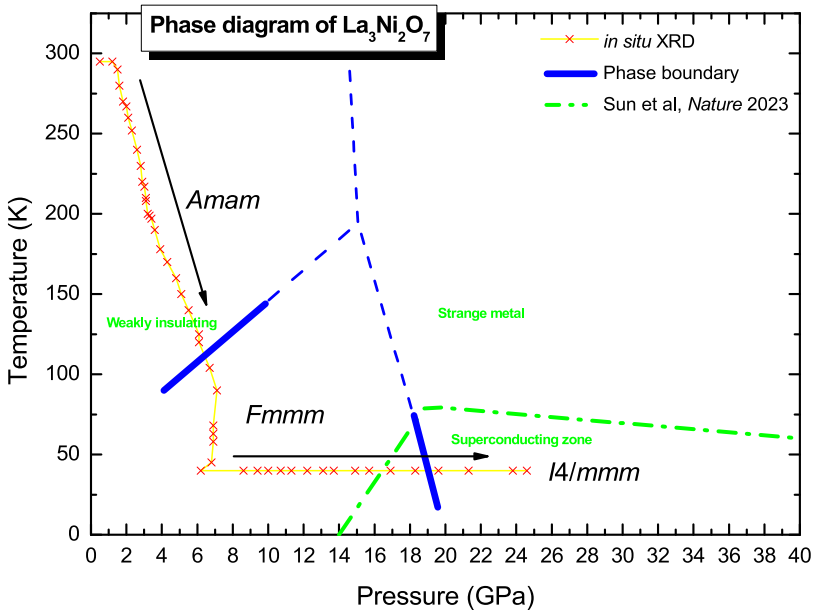

Figure 4. Phase diagram of $La_3Ni_2O_7$ based on the in situ XRD results, in which the black arrows show the path of the cooling and compression process.

https://doi.org/10.1021/jacs.3c13094
J. Am. Chem. Soc. 2024, 146, 7506−7514

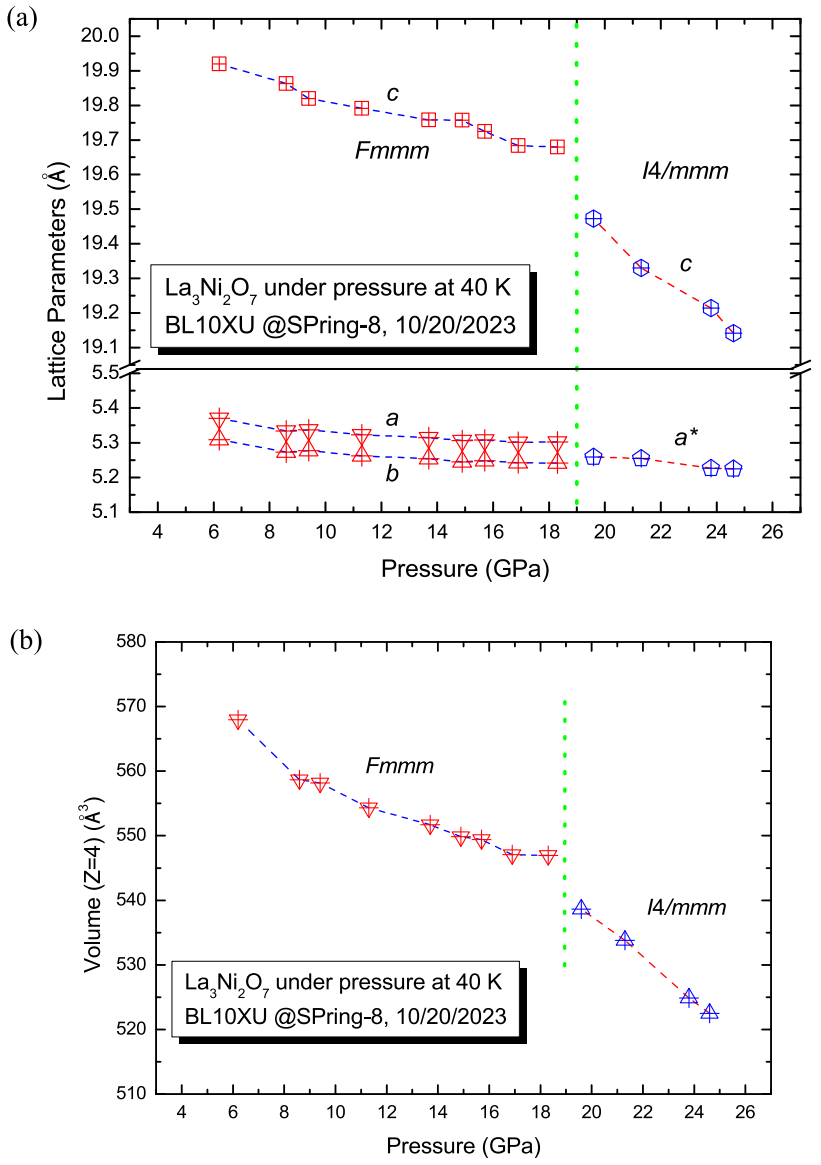

Figure 5. (a) Lattice parameters and (b) volume ($Z = 4$) as a function of pressure at 40 K, in which the reduced lattice parameter $a^* = \sqrt{2}\,a$ for the $I4/mmm$ structure.

the atomic ratio at the A site, and more smaller type atoms at the A site could stabilize the $I4/mmm$ structure.[21] Tetragonal $LaSr_2Mn_2O_7$ was observed to maintain its $I4/mmm$ structure for up to 35 GPa at room temperature.[22]

The use of smaller atoms by doping the A site in RP compounds might introduce a chemical precompression effect and make the tetragonal phase become stable at ambient conditions. However, the simulated replacement test from all rare-earth elements at the A site in $R_3Ni_2O_7$ provided the opposite results: the transition pressure from the orthorhombic structure to the tetragonal structure became significantly higher in the cases with smaller atoms at the A site.[6] The reversed suggestion, to replace A site with a bigger atom, was proposed,[7] although in these calculations, they were targeting the room-temperature structure model of the *Fmmm* structure. More calculations and experiments need to be performed to explore the effect of replacements at the A site in these RP compounds.

The lattice parameters and unit cell volume as a function of pressure are displayed in Figure 5. Table 1 summarizes the

Table 1. Lattice Parameters for the High-Pressure Phases of the $La_3Ni_2O_7$ Sample at 40 K and Various Pressure Conditions Refined from XRD Experiments and Atomic Positions Optimized Theoretically

space group: $I4/mmm$				
conditions		a (Å)	c (Å)	R_w (%)
19.6 GPa, 40 K		3.7188(8)	19.4731(4)	0.656
21.3 GPa, 40 K		3.7159(5)	19.3299(3)	0.991
23.8 GPa, 40 K		3.6957(5)	19.2145(2)	1.077
24.6 GPa, 40 K		3.6943(7)	19.1414(3)	1.152
atom	x	y	z	occ.
La1	0	0	0.3163(4)	1
La2	0	0	0.5	1
Ni	0	0	0.104(1)	1
O1	0	0.5	0.908(4)	1
O2	0	0	0.779(2)	1
O3	0	0	0	1

https://doi.org/10.1021/jacs.3c13094
J. Am. Chem. Soc. 2024, 146, 7506−7514

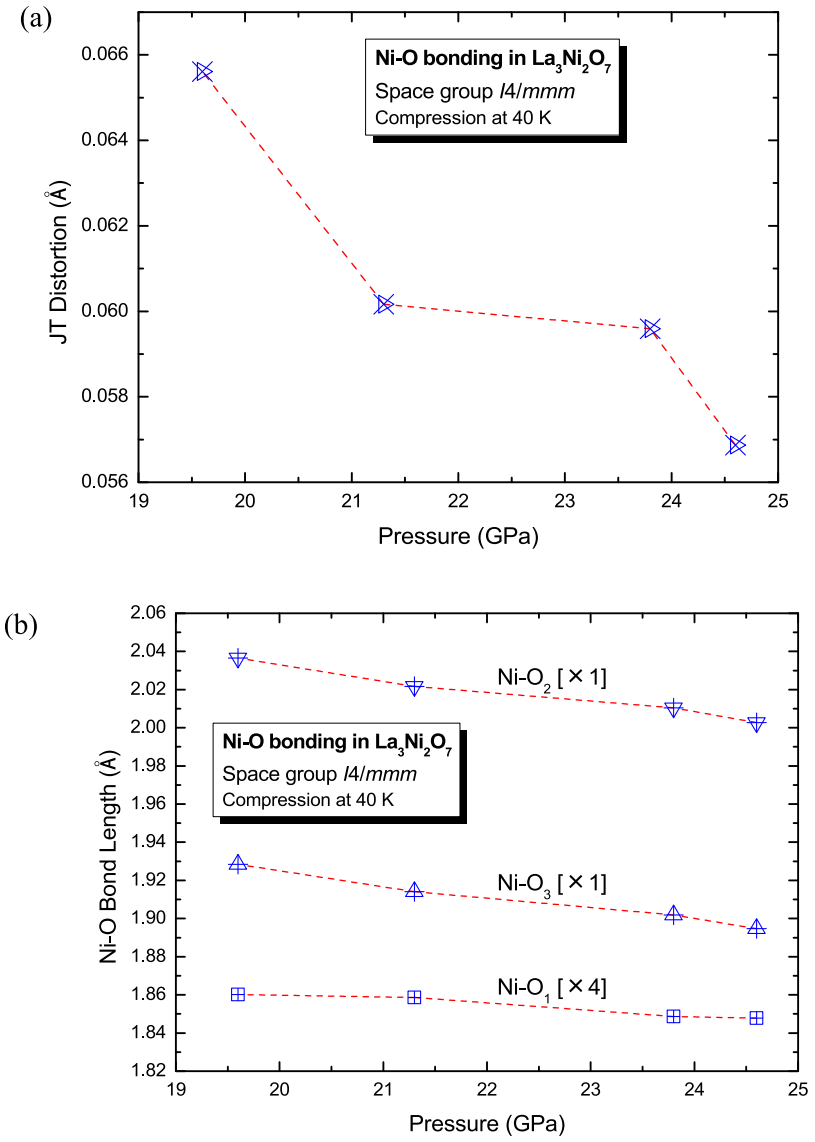

Figure 6. (a) Regularity of Ni−O octahedra, in which the JT distortion $\sigma_{JT} = [1/6\Sigma((Ni-O)_i-<Ni-O>)^2]^{1/2}$, and (b) the Ni−O bonding length in the *I*4/*mmm* structure as a function of pressure at 40 K.

lattice parameters of the *I*4/*mmm* structure from XRD Le Bail refinements and atomic positions optimized from calculations. $Z = 2$ in the *I*4/*mmm* structure and the double unit cell volume were plotted to reach $Z = 4$ for comparison with those in the *Fmmm* structure. The clear volume discontinuity could be observed with the volume drop at about 1.2% at around 19 GPa at 40 K.

The modifications of Ni−O octahedra upon compression in these RP compounds were potentially linked to the T_c trend. Figure 6, in which the JT distortion $\sigma_{JT} = [1/6\Sigma((Ni-O)_i-<Ni-O>)^2]^{1/2}$, shows that the further compression in the superconducting zone reduces the Ni−O octahedra's distortion and improves the regularity of the Ni−O octahedra. While the T_c measurement had a dropping trend with increasing pressure,[2] the elongated shape of the Ni−O octahedra, especially the longer Ni−O2 bond (as shown in Figure 3), pushed O2 atoms more to interact with the A site atom at the rock-salt type layer.

These nickelate samples were synthesized under about 10−19 bar oxygen gas pressure,[2,3] which potentially introduced extra oxygen to the sample structure, contrary to easy oxygen vacancy formation in other La−Ni−O systems synthesized without oxygen gas pressure. Most likely, similar to the $n = 1$ case in the La_2NiO_4 system,[23] extra interstitial oxygen might already get into the rock-salt type layer, which together with holes naturally plays an important role in the transport properties. However, the very recent progress on this topic reported that oxygen vacancies were visualized in the $La_3Ni_2O_{7+\delta}$ sample and were found to primarily occupy the inner apical site.[24] The effect of the oxygen vacancies needs further theoretical and experimental investigations to reveal the potential mechanism of the superconductivity.

We disclaim that the present XRD work does not confirm superconductivity in the presently studied material. Several other groups, in fact, already repeated and confirmed the superconductivity under high-pressure conditions in this same $La_3Ni_2O_7$ sample provided by the same group.[25−27]

It is noticed that another type of nickelates, the superconducting infinite-layer nickelates, exhibit an angle of 180° at in-plane Ni−O−Ni bonding angles,[28] and the correlation between T_c and these angles was proposed, since these angles directly impact the basal Ni $3d_{x^2-y^2}$ and O $2P_{x,y}$ hybridization

https://doi.org/10.1021/jacs.3c13094
J. Am. Chem. Soc. 2024, 146, 7506−7514

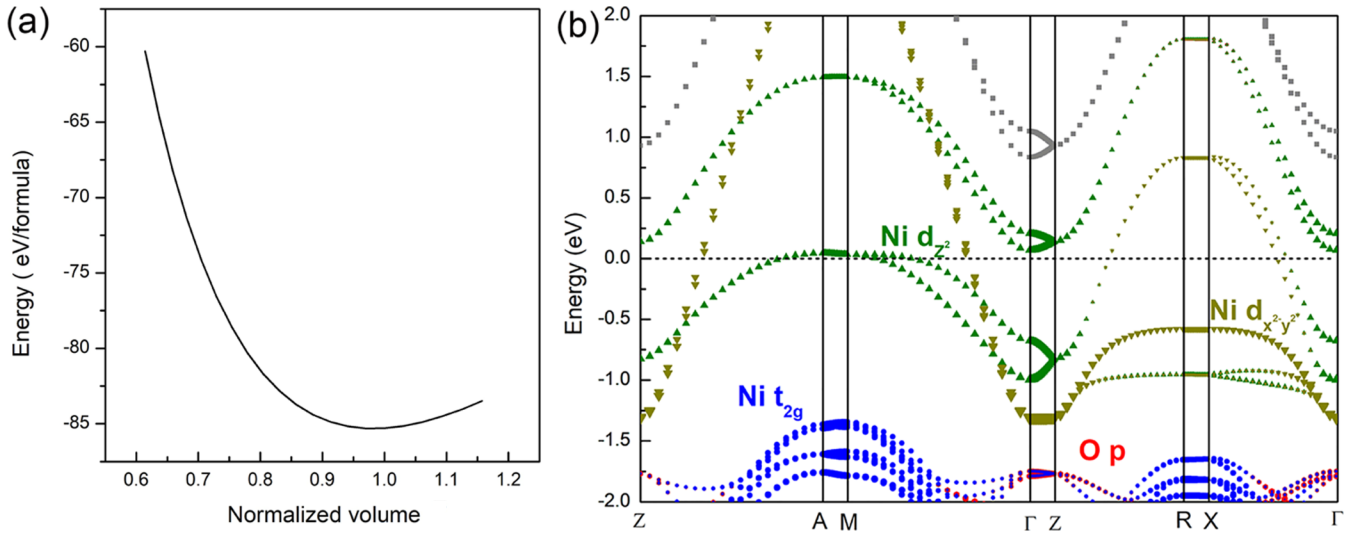

Figure 7. (a) Variation of energy with the volume of the *I4/mmm* structure. (b) Projected band structure of the *I4/mmm* structure at 20 GPa.

and then the electronic structure at the Fermi energy. Experimentally, at 19.6 GPa, this in-plane Ni−O−Ni bonding angle is 178.380° and slightly increases to 178.397° when the pressure is compressed to 24.6 GPa at 40 K in $La_3Ni_2O_7$. This is not really in favor of the proposed positive correlation for the T_c trend upon compression in this RP compound. However, attention needs to be paid to avoid overexplanation of the crystalline structural detailed information from the XRD refinement results, since the diffraction quality under two extreme conditions, high pressure and low temperature simultaneously, normally became worse compared to those obtained at ambient conditions.

The fundamental building blocks of the three structures (space group *Amam*, *Fmmm*, and *I4/mmm*) for $La_3Ni_2O_7$ in this P−T range are basically similar. However, the detailed electronic structures demonstrate slightly different features. The DFT calculations show that the *Fmmm* structure will spontaneously transform to the *I4/mmm* structure at 20 GPa without any barrier during structural relaxation. The total energy varying with the volume of the *I4/mmm* structure at 20 GPa is plotted in Figure 7a, and the projected band structure is illustrated in Figure 7b. The electronic states that approached the Fermi energy were mainly dominated by the e_g orbitals ($3d_{z^2}$ and $3d_{x^2-y^2}$) of Ni atoms, which are located in the oxygen octahedral crystal field. The Ni atoms' low energy t_{2g} orbitals ($3d_{xy}$, $3d_{yz}$, and $3d_{xz}$) in the octahedral field hybridize effectively with the 2p orbitals of oxygen and sink deeply away from the Fermi level. In order to compare the projected band structure with Fmmm phase in the previous reports, we constructed a $\sqrt{2}\times\sqrt{2}$ *I4/mmm* supercell and plotted the eigenvalues of energy in Figure S1. These results agree with previous studies in general,[2,6,7] which indicates that the Cooper pairs of superconductivity are derived from the e_g orbitals of Ni. However, the detailed mechanism of pairing should be further investigated.

In the RP-type nickelate system, when $n = 3$, a T_c of 21 K at about 70 GPa high-pressure conditions at the $La_4Ni_3O_{10}$ system was reported very recently.[29,30] These results enrich our understanding of superconductivity in RP-type nickelates. However, no in situ structure measurements at low-T and high-P conditions have been performed in the $La_4Ni_3O_{10}$ system in these reports, and again an important piece of information on the corresponding structure is missing, which is crucial for solving the mechanism puzzle. These updates, together with the previous study on this system,[31] will bring more interesting subjects to the research studies to explore the universal relationship between structure evolution and the change in properties in the RP-type La−Ni−O family at low-temperature and high-pressure conditions.

During this article review process, we found that one previous theoretical and calculation paper[32] presented that the tetragonal phase indeed was the optimized structure at high-pressure conditions in that paper's Appendix A section, which is in good agreement with our experimental and calculation results. Another very recent experimental report is also worth mentioning: the rare-earth-doping-type sample, $La_2PrNi_2O_{7-\delta}$, was discovered to have superconductivity at high-pressure conditions above 10 GPa, and the corresponding phase is a tetragonal *I4/mmm* structure.[33] Progress on the high-pressure structural study on the $La_4Ni_3O_{10}$ sample also reveals that the *I4/mmm* space group is stable under high-pressure conditions.[34] These updates further confirm our discovery of the phase responsible for superconductivity in the double-layered nickelate.

CONCLUSIONS

In summary, in situ high-pressure and low-temperature synchrotron XRD experiments were carried out, and the responsible structure in $La_3Ni_2O_7$ for its high T_c state was proposed. At 40 K, a tetragonal *I4/mmm* phase was discovered when the compression was around 19 GPa. The correlation between T_c and this structural evolution, especially Ni−O octahedra regularity and the in-plane Ni−O−Ni bonding angles, was discussed. This updated phase diagram based on XRD results will help us better understand the mechanism of this unconventional high T_c superconductor in $La_3Ni_2O_7$ and offer relatively clear guidelines to synthesize related compound systems and potentially eventually realize the superconducting state at ambient conditions instead of at high-pressure conditions.

https://doi.org/10.1021/jacs.3c13094
J. Am. Chem. Soc. 2024, 146, 7506−7514

■ ASSOCIATED CONTENT

Supporting Information

The Supporting Information is available free of charge at https://pubs.acs.org/doi/10.1021/jacs.3c13094.

Projected band structure at $\sqrt{2}\times\sqrt{2}$ $I4/mmm$ supercell (PDF)

Accession Codes

CCDC 2309451 and 2327364−2327366 contain the supplementary crystallographic data for this paper. These data can be obtained free of charge via www.ccdc.cam.ac.uk/data_request/cif, or by emailing data_request@ccdc.cam.ac.uk, or by contacting The Cambridge Crystallographic Data Centre, 12 Union Road, Cambridge CB2 1EZ, U.K.; fax: +44 1223 336033.

■ AUTHOR INFORMATION

Corresponding Authors

Luhong Wang − *Shanghai Key Laboratory of Material Frontiers Research in Extreme Environments, Shanghai Advanced Research in Physical Sciences, Shanghai 201203, China*; orcid.org/0000-0001-8851-4935; Email: lisaliu@sharps.ac.cn

Meng Wang − *Center for Neutron Science and Technology, Guangdong Provincial Key Laboratory of Magnetoelectric Physics and Devices, School of Physics, Sun Yat-Sen University, Guangzhou, Guangdong 510275, China*; Email: wangmeng5@mail.sysu.edu.cn

Haozhe Liu − *Center for High Pressure Science & Technology Advanced Research, Beijing 100094, China*; orcid.org/0000-0001-5720-2031; Email: haozhe.liu@hpstar.ac.cn

Authors

Yan Li − *State Key Lab of Superhard Materials, College of Physics, Jilin University, Changchun 130012, China*; orcid.org/0000-0002-1401-7925

Sheng-Yi Xie − *School of Physics and Electronics, Hunan University, Changsha 410082, China*; orcid.org/0000-0002-9369-0914

Fuyang Liu − *Center for High Pressure Science & Technology Advanced Research, Beijing 100094, China*

Hualei Sun − *School of Sciences, Sun Yat-Sen University, Guangzhou, Guangdong 510275, China*

Chaoxin Huang − *Center for Neutron Science and Technology, Guangdong Provincial Key Laboratory of Magnetoelectric Physics and Devices, School of Physics, Sun Yat-Sen University, Guangzhou, Guangdong 510275, China*

Yang Gao − *Center for High Pressure Science & Technology Advanced Research, Beijing 100094, China*

Takeshi Nakagawa − *Center for High Pressure Science & Technology Advanced Research, Beijing 100094, China*; orcid.org/0000-0001-6283-8755

Boyang Fu − *School of Materials and Energy, University of Electronic Science and Technology of China, Chengdu, Sichuan 611731, China*

Bo Dong − *Harbin Institute of Technology, Harbin 150001, China*

Zhenhui Cao − *State Key Lab of Superhard Materials, College of Physics, Jilin University, Changchun 130012, China*

Runze Yu − *Center for High Pressure Science & Technology Advanced Research, Beijing 100094, China*

Saori I. Kawaguchi − *Japan Synchrotron Radiation Research Institute, Sayo-gun Hyogo 679-5198, Japan*

Hirokazu Kadobayashi − *Japan Synchrotron Radiation Research Institute, Sayo-gun Hyogo 679-5198, Japan*

Changqing Jin − *Beijing National Lab for Condensed Matter Physics, Institute of Physics, Chinese Academy of Sciences, Beijing 100190, China*

Ho-kwang Mao − *Center for High Pressure Science & Technology Advanced Research, Beijing 100094, China; Shanghai Advanced Research in Physical Sciences, Shanghai 201203, China*

Complete contact information is available at: https://pubs.acs.org/10.1021/jacs.3c13094

Notes

The authors declare no competing financial interest.

■ ACKNOWLEDGMENTS

This work was supported by the Natural Science Foundation of China (11374075, 12174454, 11704111, 2023YFA140600, 11921004, and U2032220). The authors acknowledge financial support from the Shanghai Science and Technology Committee, China (No. 22JC1410300) and Shanghai Key Laboratory Novel Extreme Condition Materials, China (No. 22dz2260800). Work at SYSU was supported by Guangdong Basic and Applied Basic Research Funds (grant no. 2021B1515120015), Guangzhou Basic and Applied Basic Research Funds (grant no. 202201011123, 2024A04J6417), and Guangdong Provincial Key Laboratory of Magnetoelectric Physics and Devices (grant no. 2022B1212010008). Calculation resources were provided by the National Supercomputing Center in Shenzhen (Shenzhen Cloud Computing Center).

■ REFERENCES

(1) Hosoya, T.; Igawa, K.; Takeuchi, Y.; Yoshida, K.; Uryu, T.; Hirabayashi, H.; Takahashi, h. Pressure studies on the electrical properties in $R_{2-x}Sr_xNi_{1-y}Cu_yO_{4+\delta}$ (R = La, Nd) and $La_3Ni_2O_{7+\delta}$. *J. Phys.: Conf. Ser.* **2008**, *121*, No. 052013.

(2) Sun, H.; Huo, M.; Hu, X.; Li, J.; Liu, Z.; Han, Y.; Tang, L.; Mao, Z.; Yang, P.; Wang, Bo.; Cheng, J.; Yao, D.-X.; Zhang, G.-M.; Wang, M. Signature of superconductivity near 80 K in a nickelate under high pressure. *Nature* **2023**, *621*, 493−498, DOI: 10.1038/s41586-023-06408-7.

(3) Liu, Z.; Sun, H.; Huo, M.; Ma, X.; Ji, Y.; Yi, E.; Li, L.; Liu, H.; Yu, J.; Zhang, Z.; Chen, Z.; Liang, F.; Dong, H.; Guo, H.; Zhong, D.; Shen, B.; Li, S.; Wang, M. Evidence for charge and spin density waves in single crystals of $La_3Ni_2O_7$ and $La_3Ni_2O_6$. *Sci. China: Phys., Mech. Astron.* **2023**, *66*, No. 217411, DOI: 10.1007/s11433-022-1962-4.

(4) Luo, Z.; Hu, X.; Wang, M.; et al. Bilayer tow-orbital model of $La_3Ni_2O_7$ under pressure. *Phys. Rev. Lett.* **2023**, *131*, No. 126001, DOI: 10.1103/physrevlett.131.126001.

(5) Zhang, Y.; Lin, L.-F.; Moreo, A.; Maier, T. A.; Dagotto, E. Trends in electronic structures and s±-wave pairing for the rare-earth series in bilayer nickelate superconductor R3Ni2O7. *Phys. Rev. B* **2023**, *108*, No. 165141, DOI: 10.1103/physrevb.108.165141.

(6) Geisler, B.; Hamlin, J. J.; Stewart, G. R.; Hennig, R. G.; Hirschfeld, P. J. Structural transitions, octahedral rotations, and electronic properties of $A_3Ni_2O_7$ rare-earth nickelates under high pressure. 2023 arXiv:2309.15078. arXiv.org e-Print archive. https://arxiv.org/abs/2309.15078.

(7) Rhodes, L. C.; Wahl, P. Structural routes to stabilize superconducting $La_3Ni_2O_7$ at ambient pressure 2023 arXiv:2309.15745. arXiv.org e-Print archive. https://arxiv.org/abs/2309.15745.

(8) Anderson, O. L.; Isaak, D. G.; Yamamoto, S. Anharmonicity and the equation of state for gold. *J. Appl. Phys.* **1989**, *65*, 1534−1543, DOI: 10.1063/1.342969.
(9) Dorogokupets, P. I.; Dewaele, A. Equations of state of MgO, Au, Pt, NaCl-B1, and NaCl-B2: internally consistent high-temperature pressure scale. *High Pressure Res.* **2007**, *27*, 431−446, DOI: 10.1080/08957950701659700.
(10) Tsuchiya, Taku.First-principles prediction of the P-V-T equation of state of gold and the 660-km discontinuity in Earth's mantle *J. Geophys. Res.* 2003, *108*(B10), 2462 DOI: 10.1029/2003JB002446.
(11) Prescher, C.; Prakapenka, V. B. DIOPTAS: a program for reduction of two-dimensional X-ray diffraction data and data exploration. *High Pressure Res.* **2015**, *35* (3), 223−230, DOI: 10.1080/08957959.2015.1059835.
(12) Toby, B. H.; Von Dreele, R. B. GSAS-II: the genesis of a modern open-source all purpose crystallography software package. *J. Appl. Crystallogr.* **2013**, *46* (2), 544−549, DOI: 10.1107/S0021889813003531.
(13) Kresse, G.; Furthmüller, J. Efficient iterative schemes for *ab initio* total-energy calculations using a plane-wave basis set. *Phys. Rev. B* **1996**, *54*, No. 11169, DOI: 10.1103/PhysRevB.54.11169.
(14) Blöchl, P. E. Projector augmented-wave method. *Phys. Rev. B* **1994**, *50*, No. 17953, DOI: 10.1103/PhysRevB.50.17953.
(15) Perdew, J. P.; Burke, K.; Ernzerhof, M. Generalized gradient approximation made simple. *Phys. Rev. Lett.* **1996**, *77*, No. 3865, DOI: 10.1103/PhysRevLett.77.3865.
(16) Ruddlesden, S. N.; Popper, P. The compound $Sr_3Ti_2O_7$ and tis structure. *Acta Crystallogr.* **1958**, *11*, 54−55, DOI: 10.1107/S0365110X58000128.
(17) Harris, A. B. Landau theory of tilting of oxygen octahedra in perovskite. *Phys. Rev. B* **2012**, *85*, No. 174107.
(18) Yatoo, M. A.; Skinner, S. J. Ruddlesden-Popper phase materials for solid oxide fuel cathodes: A short review. *Mater. Today: Proc.* **2022**, *56*, 3747−3754, DOI: 10.1016/j.matpr.2021.12.537.
(19) Zhang, Z.; Greenblatt, M.; Goodenough, J. B. Synthesis, structure and properties of the layered perovskite $La_3Ni_2O_{7-\delta}$. *J. Solid State Chem.* **1994**, *108*, 402−409, DOI: 10.1006/jssc.1994.1059.
(20) Ling, C. D.; Argyriou, D. N.; Wu, G.; Neumeier, J. J. Neutron diffraction study of $La_3Ni_2O_7$: Structure relationships among n = 1, 2, and 3 phase $La_{n+1}Ni_nO_{3n+1}$. *J. Solid State Chem.* **1999**, *152*, 517−525, DOI: 10.1006/jssc.2000.8721.
(21) Ling, C. D.; Millburn, J. F.; Mitchell, J. F.; Argyriou, D. N.; Linton, J.; Bordallo, H. N. Interplay of spin and orbital ordering in the layered colossal magnetoresistance Manganite $La_{2-2x}Sr_{1+2x}Mn_2O_7$ ($0.5 < x < 1.0$). *Phys. Rev. B* **2000**, *62*, No. 15096, DOI: 10.1103/PhysRevB.62.15096.
(22) Kumar, R. S.; Prabhakaran, D.; Boothroyd, A.; Nicol, M. F.; Cornelius, A. High pressure structure of $LaSr_2Mn_2O_7$ bilayer Manganite. *J. Phys. Chem. Solids* **2006**, *67*, 2046−2050, DOI: 10.1016/j.jpcs.2006.05.029.
(23) Nakamura, T.; Oike, R.; Ling, Y.; Tamenori, Y.; Amezawa, K. The determining factor for interstitial oxygen formation in Ruddlesden-Popper type La_2NiO_4-base oxides. *Phys. Chem. Chem. Phys.* **2016**, *18*, 1564−1569, DOI: 10.1039/c5cp05993c.
(24) Dong, Z.; Huo, M.; Li, J.; Li, J.; Li, P.; Sun, H.; Lu, Y.; Wang, M.; Wang, Y.; Chen, Z. Visualization of oxygen vacancies and self-doped ligand holes in $La_3Ni_2O_{7+\delta}$. 2023. arXiv:2312.15727. arXiv.org e-Print archive. https://arxiv.org/abs/2312.15727.
(25) Hou, J.; Yang, P.-T.; Liu, Z.-Y.; Li, J.-Y.; Shan, P.-F.; Ma, L.; Wang, G.; Wang, N.-N.; Guo, H.-Z.; Sun, J.-P.; Uwatoko, Y.; Wang, M.; Zhang, G.-M.; Wang, B.-S.; Cheng, J.-G. Emergence of High-Temperature. Superconducting Phase in Pressurized $La_3Ni_2O_7$ Crystals. *Chin. Phys. Lett.* **2023**, *40*, No. 117302.
(26) Zhang, Y.; Su, D.; Huang, Y.; Sun, H.; Huo, M.; Shan, Z.; Ye, K.; Yang, Z.; Li, R.; Smidman, M.; Wang, M.; Jiao, L.; Yuan, H. High-temperature superconductivity with zero-resistance and strange metal behavior in $La_3Ni_2O_7$. 2023 arXiv:2307.14819. arXiv.org e-Print archive. https://arxiv.org/abs/2307.14819.
(27) Sun, L.; Zhou, Y.; Guo, J.; Cai, S.; Wang, P.; Han, J.; Chen, X.; Wu, Q.; Ding, Y.; Xiang, T.; Mao, H.-k. Evidence of filamentary superconductivity in pressurized $La_3Ni_2O_{7\text{-delta}}$ single crystals. 2023. arXiv:2311.12361. arXiv.org e-Print archive. https://arxiv.org/abs/2311.12361.
(28) Li, D.; Lee, K.; Wang, B. Y.; Osada, M.; Crossley, S.; Lee, H. R.; Cui, Y.; Hikita, Y.; Hwang, H. Y. Superconductivity in an infinite-layer nickelate. *Nature* **2019**, *572*, 624−627, DOI: 10.1038/s41586-019-1496-5.
(29) Zhang, M.; Pei, C.; Du, X.; Cao, Y.; Wang, Q.; Wu, J.; Li, Y.; Zhao, Y.; Li, C.; Cao, W.; Zhu, S.; Zhang, Q.; Yu, N.; Cheng, P.; Zhao, J.; Chen, Y.; Guo, H.; Yang, L.; Qi, Y. Superconductivity in trilayer nickelate $La_4Ni_3O_{10}$ under pressure. 2023 arXiv:2311.07423. arXiv.org e-Print archive. https://arxiv.org/abs/2311.07423.
(30) Li, Q.; Zhang, Y.-J.; Xiang, Z.-N.; Zhang, Y.; Zhu, X.; Wen, H.-H. Signature of superconductivity in pressurized $La_4Ni_3O_{10}$. 2023 arXiv:2311.05453. arXiv.org e-Print archive. https://arxiv.org/abs/2311.05453.
(31) Li, H.; Zhou, X.; Nummy, T.; Zhang, J.; Pardo, V.; Pickett, W. E.; Mitchell, J. F.; Dessau, D. S. Fermiology and electron dynamics of trilayer nickelate $La_4Ni_3O_{10}$. *Nat. Commun.* **2017**, *8*, No. 704, DOI: 10.1038/s41467-017-00777-0.
(32) LaBollita, H.; Pardo, V.; Norman, M. R.; Botana, A. S. Electronic structure and magnetic properties of $La_3Ni_2O_7$ under pressure. 2023 arXiv:2309.17279. arXiv.org e-Print archive. https://arxiv.org/abs/2309.17279.
(33) Wang, G.; Wang, N.; Wang, Y.; Shi, L.; Shen, X.; Jun, H.; Ma, H.; Yang, P.; Liu, Z.; Zhang, H.; Dong, X.; Sun, J.; Wang, B.; Jiang, K.; Hu, J.; Uwatoko, Y.; Cheng, J. Observation of high-temperature superconductivity in the high-pressure tetragonal phase of $La_2PrNi_2O_{7-\delta}$. 2023 arXiv:2311.08212. arXiv.org e-Print archive. https://arxiv.org/abs/2311.08212.
(34) Li, J.; Chen, C.; Huang, C.; Han, Y.; Huo, M.; Huang, X.; Ma, P.; Qiu, Z.; Chen, J.; Hu, X.; Chen, L.; Xie, T.; Shen, B.; Sun, H.; Yao, D.; Wang, M. Structural transiton and electronic band structures in the compressed trilayer nickelate $La_4Ni_3O_{10}$. 2023 arXiv:2311.16763. arXiv.org e-Print archive. https://arxiv.org/abs/2311.16763.